Scientific Research Publishing

International Journal of Geosciences, 2022, 13, 918-935
https://www.scirp.org/journal/ijg
ISSN Online: 2156-8367
ISSN Print: 2156-8359

Petrology, Structural and Geochemistry of the Copper-Nickle-Iron Bearing Rocks in Korr-Marsabit Area, Northern Kenya

Aaron K. Waswa

Department of Earth and Climate Sciences, Faculty of Science and Technology, University of Kenya, Nairobi, Kenya
Email: awaswa@uonbi.ac.ke

How to cite this paper: Waswa, A.K. (2022) Petrology, Structural and Geochemistry of the Copper-Nickle-Iron Bearing Rocks in Korr-Marsabit Area, Northern Kenya. *International Journal of Geosciences*, **13**, 918-935.
https://doi.org/10.4236/ijg.2022.1310046

Received: September 18, 2022
Accepted: October 28, 2022
Published: October 31, 2022

Abstract

The main objective of this study was to investigate copper-Nickle-Iron bearing rocks of the northern Kenya, and understand their mode of formation. The area of study is bounded by latitudes 2˚52'00"N and 1˚52'00"N and longitudes 37˚19'00"E and 37˚36'00"E, South West of Marsabit town. The methods involved geological field mapping between September, 2020 and December 2020. Elemental analyses of the samples were done using an XRF. Pearsonian correlation on the analyzed elements was done using Oasis Montaj 8.4. Fabric8 software was used to analyze structural data. The area comprises metamorphic, igneous and sedimentary rocks. Metamorphic rocks include biotite hornblende gneisses, biotite gneisses, biotite muscovite gneisses and marbles. Basalts of different mineralogy were also found in the area. Colluvium and alluvium sediments were found covering some of the metamorphic rocks in some areas. Malachite occurs in gneisses in the central part of the area. The area has undergone deformation, which includes jointing and folding. The fold axis trend in the North-South direction and plunges to the southern part of the area. Correlation of the elements shows that there is a positive correlation of Copper-Nickel-Iron. This indicates similar mode of delivery within the host rocks. Kriging indicates spatial distribution of these elements within the study area. The average size of distribution can easily be computed from the maps produced by kriging.

Keywords

Petrology, Structural Geology, Geochemistry, Copper-Nickel-Iron, Kriging

1. Introduction

Marsabit County comprises medium to high grade metamorphic rocks igneous

rocks and some sedimentary rocks Charsley [1]. Key [2] has briefly discussed some of these rocks. Metamorphic rocks within the area belong to the rocks of East African orogenesis which has been discussed by Stern [3] and Key [4]. Waswa *et al.* [5] made elaborative discussion on the formation of Neoproterozoic metamorphic rocks of Kenya. Most rocks in this area follow the general trend of metamorphic rocks in the Mozambique mobile belt (Mathu [6]; Mathu [7]; Mathu [8]; Nyamai *et al.*, [9], 1993; Waswa *et al.* [5]; Nyamai *et al.*, [10]). The study area is in Marsabit county, Korr area. This area occurs to the northern part of Kenya and represents an important metallogenic province with Copper-Nickel-Iron deposit. Apart from Copper-Nickel-Iron deposits, other minerals found in the area include; Chromite, Manganese and Titanium. The area comprises medium to high grade metamorphic rocks and volcanics.

The area is bounded by latitudes 2˚52'00"N and 1˚52'00"N and longitudes 37˚19'00"E and 37˚36'00"E, south west of Marsabit town. The area can be accessed from Nairobi-Nanyuki-Marsabit road (**Figure 1**). This road is tarmacked and passable in all weather. Road network within the area of the licensed is good only that all the roads are not tarmacked. Mobile network for Safaricom and Airtell are available within the area.

The area has a marked contrast of landforms between high mountains and rolling low lands. The western part exhibits low land terrain while mountainous terrain is observed on the eastern part of the area. Meandering watercourses are observed in the lowlands. The mountainous areas have linear watercourses with short tributaries that follow maximum slopes of the hills. Semi-arid vegetation occurs in the area. Most trees are being acacia and some cactus. The main activity in the area is pastoralism, which involves keeping of cattle, goats, sheep, donkeys and camels.

The genesis of Cu-Ni-Fe has been a subject of concern to most exploration geologist. Most concepts have been coined to magmatic systems (Clark, [11]; Clark [12]; Distler and Genkin [13]; Distler *et al.*, [14] [15]). The enigma of the occurrence of this minerals in metamorphic terrane has been of great interest to most geologists. This paper attempts to investigate this paradox of the occurrence of Cu-Ni-Fe within the metamorphic terrane in Kenya.

2. Geological Setting of Korr-Marsabit Area

Korr-Marsabit area is composed of metamorphic rocks, igneous rocks and sedimentary deposits. The eastern part of the area is unconformably overlain by Marsabit volcanic shield (Key, [2]). This volcanic shield consists of the basalts of Mio-Pliocene according to Key [2]. Basalts occupy the eastern part of the area (**Figure 1**). They are horizontal and were deposited on planar surfaces. The metamorphic rocks consists of mica gneisses, migmatites, granitoid gneisses, and the marbles. Mica gneisses is a group of gneisses that includes: Biotite hornblende gneisses, biotite muscovite gneisses, and biotite gneisses.

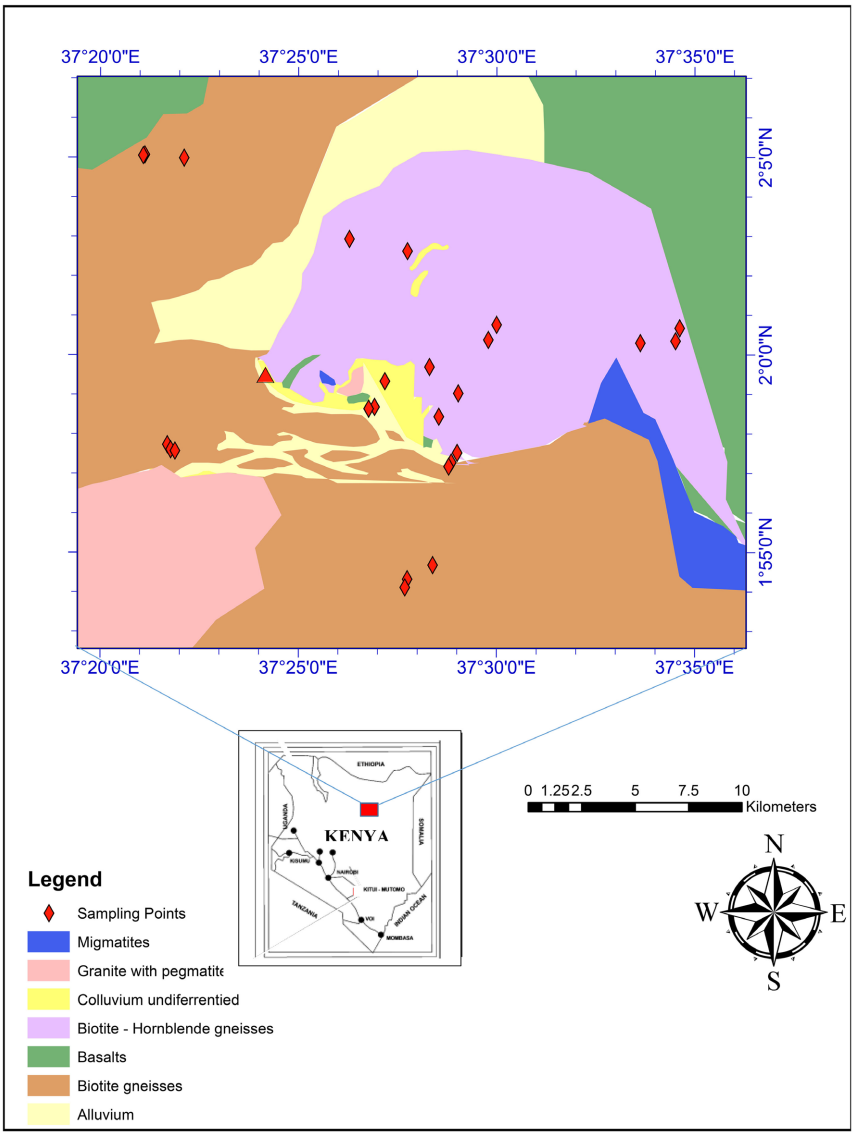

Figure 1. Geological Map of Korr-Marsabit area, Northern part of Kenya.

2.1. Biotite-Hornblende Gneisses

Biotite hornblende gneisses were encountered at station BR/001 whose coordinates are northings 331362 and eastings of 219351 at an elevation of 566 meters above sea level. They are coarse grained and have dark shiny minerals (biotite) and long dark hornblende minerals. The biotite-hornblende gneisses are melanocratic, foliated and jointed (**Figure 2**).

Sample BR/002A and BR/002B contain malachite (**Figure 3**). These samples were collected in a pit of about 3m deep. The coordinates of the area sampled are 0330458 northings and 0218259 at an altitude of 570 meters above sea level. The rocks have the surface which altered to reddish brown colour. While fresh samples are melanocratic. Minerals present include; biotite, hornblende and copper (malachite and azurite) (see **Table 1**). These gneisses have discrete foliation where felsic minerals alternates with mafic minerals.

Figure 2. Biotite hornblende gneisses (BR/002A). The hammer handle (30 cm) is used as the scale.

Figure 3. Biotite hornblende gneisses (BR/001). The hammer handle (30 cm) is used as the scale.

Table 1. Modal composition of Hornblende biotite gneisses.

Mineral	BR/001 (Vol. %)	BR/002A (Vol. %)	BR/002B (Vol. %)
Quartz	**20**	**15**	**15**
Plagioclase	**20**	**10**	**10**
Biotite	**30**	**20**	**15**
Hornblende	**25**	**15**	**15**
Malachite	-	**35**	**40**
Accessory	**5**	**5**	**5**

2.2. Biotite-Muscovite Gneisses

Biotite muscovite gneisses were encountered at station BR/006 whose coordinates are 0330018/0220586. The altitude is 598 meters above sea level. These rocks are foliated (Figure 4) and trend in the NE-SW direction. The modal composition of the minerals of these rocks is indicated in Table 2.

2.3. Biotite Gneisses

Biotite gneisses were mapped at station BR/008, whose coordinates are 0326274/

0226558. The altitude is 567 above sea level. Leucocratic minerals are Quartz and feldspar minerals (Table 3) which are visible in hand specimen. Melanocratic minerals include with biotite and magnetite. This rocks are highly jointed (Figure 5). These rocks Dip at an angle of 40˚, to the south east with a strike of 320˚SW (Figure 6).

2.4. Marbles and Calcrete

Boulders of marbles which are well rounded were observed at station BR/013 (0317903/0216746). These marbles are within biotite gneisses. The altitude is 619meter above sea level. They are White in colour (Figure 7), but have inclusions of biotite in some areas. Calcrete limestones (Figure 8) occur at station BR/012, whose coordinates are 0317750/0216983.

Table 2. Modal composition of Biotite-Muscovite gneisses.

Mineral	BR/006 (Vol. %)	BR/0007(Vol. %)
Quartz	30	35
Plagioclase	30	30
Biotite	15	10
Muscovite	20	20
Accessory	5	5

Table 3. Modal composition of Biotite gneisses.

Mineral	BR/008 (Vol. %)	BR/0017 (Vol. %)	BR/024 (Vol. %)
Quartz	20	20	25
Plagioclase	65	50	45
Biotite	10	25	25
Hornblende	-	-	-
Accessory	5	5	5

Figure 4. Biotite Muscovite gneisses. The hammer handle (30 cm) is used as the scale.

Figure 5. Biotite gneisses (BR/008). The hammer handle (30 cm) is used as the scale.

Figure 6. Biotite gneisses (BR/024). The hammer handle (30 cm) is used as the scale.

Figure 7. Marble within Biotite gneisses. The hammer handle (30 cm) is used as the scale.

Figure 8. Calcrete limestone BR/012. The hammer handle (30 cm) is used as the scale.

2.5. Pegmatites

Two types of pegmatites were encountered during the fieldwork in the area, quartz pegmatites and quartz feldspar pegmatites. These pegmatites cut across the metamorphic rocks.

Quartz pegmatites

These pegmatites occur on the southern part of the area (**Figure 9**). Most of them cut across the biotite gneisses. They are white, though some pegmatites have grey coloured quartz with iron stains.

Quartz feldspar pegmatites

Quartz feldspar pegmatites were observed also occurring in the biotite gneisses (**Figure 10**). They cut across the host rocks and trend in the north-south direction. The minerals composition of these pegmatites is feldspar and quartz.

2.6. Migmatites and Granitoid Gneisses

Migmatites and granitoid gneisses occur in the central and southern part of the area. Distinction between granitoid gneisses and migmatites was made in the field rather than in the laboratory. Migmatites contain distinctive bands of paleo-somes and neo-somes. Paleo-somes consists of biotite minerals and hornblende while neo-somes consists of quartz and feldspars. Granitoid gneisses have more of the porphyroblastic feldspars compared to the migmatites. Mehnert [16] describes migmatites as rocks with a mixture of old and new components (**Figure 11**). Waswa [5] discussed this kind of rocks in Mutomo-Ikutha area. Granitoid gneisses (**Figure 12**) are high grade metamorphic rocks. They appear to have medium to fine grains unlike the migmatites. Their main minerals are quartz, feldspar and biotite.

Figure 9. Quartz feldspar Pegmatite. The hammer handle (30 cm) is used as the scale.

Figure 10. Quartz Pegmatite. The hammer handle (30 cm) is used as the scale.

Figure 11. Migmatites (0328996/0225984/562). The hammer handle (30 cm) is used as the scale.

Figure 12. Granitoid gneisses (0306954/0206487/738). The hammer handle (30 cm) is used as the scale.

2.7. Basalts

Greenish-grey basalts (**Figure 13**) were found in station BR/009 at northings 0324836 and eastings of 0279607. They contain magnetite, feldspar and some quartz minerals. Basalt were found overlying metamorphic rocks at some places as seen **Figure 14**. Other areas where basalts were observed are stations BR/16 of the coordinates 0341539/0221781 and BR/018: Olivine basalts of coordinates 0339889/0221687.

3. Structural and Tectonics of Korr Area

Korr area lies in the east African orogeny. The name East African orogeny was proposed by Stern [3]. The process of formation involved break up, formation of the ocean floor and collision of the east and west godwanaland (Biyajima *et al.*, [17]). The signatures of these deformation is observed in the metamorphosed rocks. Foliation planes that were measured and analyzed indicate that the principal stress components were involved. Sigma 1 principal stress operated in the east-west direction, while minimum stress was in the North-South direction. These process resulted into folding as depicted by the Figure below. **Figure 15** and **Figure 16** readings were mainly taken on biotite gneisses and hornblende biotite gneisses found in the area. These rocks were also found to be hosting copper ore. Most rocks dip to the west while a few of them dip to the East. From the diagram, it is observed the fold axial plane and its axis is in the NNW-SSE direction. It can also be noted that the fold axis is plunging, which is an indication of non-cylindrical folds.

4. Geochemical Analysis

Samples from the field were analysed using X-Ray Fluorescence. The first set of the analysis was done on 24 samples (**Table 4**). This analysis was carried out before krigging. The second set of analysis was done based on the kriging that had been done on the first set. The second set of analysis comprised four samples (**Table 5**).

Table 4. Analytical results done using XRF on the first set of samples.

	NO.	MgO (Wt%)	Al_2O_3 (Wt%)	SiO_2 (Wt%)	P_2O_5 (Wt%)	S (Wt%)	K_2O (Wt%)	CaO (Wt%)	Ti (Wt%)	V (Wt%)	Cr (Wt%)	Mn (Wt%)	Fe (Wt%)	Co (Wt%)	Ni (Wt%)	Cu (Wt%)
1	BR/002B	11.152	8.728	50.747	0.146	0.481	1.005	8.429	0.655	0.013	0.146	0.101	12.607	0.002	2.419	3.227
2	BR/002A	12.459	7.416	54.957	0.062	0.159	0.411	10.951	0.677	0.013	0.111	0.100	9.269	0.000	0.822	2.462
3	BR/002E	13.683	5.720	49.451	0.207	0.430	0.681	9.960	0.533	0.011	0.160	0.103	13.373	0.000	1.740	3.775
4	BR/004BA	33.209	3.487	55.040	0.000	0.037	0.040	1.260	0.039	0.008	0.236	0.158	6.307	0.008	0.140	0.018
5	BR/004B	33.945	3.046	54.848	0.000	0.038	0.028	1.258	0.037	0.008	0.229	0.159	6.225	0.007	0.142	0.017
6	BR/013	1.758	26.240	63.590	0.080	0.080	0.235	7.409	0.028	0.000	0.017	0.006	0.382	0.000	0.001	0.003
7	BR/009	3.644	17.445	59.619	0.690	0.008	0.785	9.700	1.242	0.000	0.000	0.105	6.430	0.000	0.011	0.020
8	BR/021	46.277	2.353	43.553	0.048	0.025	0.045	1.896	0.004	0.006	0.137	0.118	5.275	0.009	0.194	0.005
9	BR/024	1.694	23.345	63.820	0.005	0.193	10.124	0.411	0.007	0.014	0.033	0.033	0.089	0.000	0.001	0.002
10	BR/011S	2.252	4.158	90.887	0.129	0.084	0.503	1.118	0.159	0.000	0.015	0.012	0.576	0.000	0.000	0.001
11	BR/26S	5.311	15.111	68.420	0.675	0.099	2.928	4.486	0.366	0.000	0.008	0.058	2.297	0.000	0.001	0.002
12	BR/015	0.000	8.626	48.235	0.680	1.497	1.285	23.150	0.529	0.026	0.006	0.155	7.858	0.000	0.003	0.011
13	BR/029S	0.000	10.803	69.463	0.364	0.140	1.202	10.488	0.640	0.000	0.000	0.172	6.626	0.000	0.002	0.005
14	BR/105	3.093	7.891	83.666	0.064	0.082	1.217	2.367	0.291	0.000	0.000	0.021	1.190	0.000	0.000	0.001
15	BR/019	9.642	9.247	69.752	0.430	0.270	2.073	4.498	0.475	0.000	0.000	0.079	3.203	0.000	0.016	0.005
16	BR/001	7.853	10.032	46.480	0.099	0.797	0.188	25.202	0.928	0.000	0.000	0.047	7.983	0.000	0.033	0.025
17	BR/20	22.755	5.065	48.360	0.000	0.676	0.000	16.113	0.677	0.048	0.052	0.120	5.674	0.000	0.199	0.038
18	BR/017	7.068	21.345	49.288	0.452	0.070	0.043	18.486	0.059	0.000	0.048	0.037	2.492	0.000	0.198	0.034
19	BR/027	5.617	20.765	57.364	0.365	0.000	0.456	8.695	0.714	0.000	0.000	0.091	5.844	0.004	0.017	0.008
20	BR/006	31.614	12.344	41.674	0.000	0.064	6.030	0.804	0.638	0.000	0.016	0.035	6.148	0.000	0.212	0.006
21	BR/22B	45.949	2.055	40.143	0.040	0.170	0.000	2.773	0.032	0.000	0.148	0.005	7.510	0.000	1.053	0.039
22	BR/016	44.304	14.836	39.063	0.074	0.015	0.186	0.565	0.076	0.005	0.003	0.143	0.607	0.000	0.004	0.005
23	BR/004	24.874	6.601	46.351	0.000	1.745	0.793	11.032	0.986	0.000	0.000	0.149	6.463	0.000	0.286	0.151
24	BR/003	15.068	17.361	54.635	0.476	0.000	3.411	4.168	0.654	0.000	0.000	0.009	3.674	0.000	0.40	0.003

Table 5. Analytical results of the second set of samples.

	NO.	MgO (Wt%)	Al_2O_3 (Wt%)	SiO_2 (Wt%)	P_2O_5 (Wt%)	S (Wt%)	K_2O (Wt%)	CaO (Wt%)	Ti (Wt%)	V (Wt%)	Cr (Wt%)	Mn (Wt%)	Fe (Wt%)	Co (Wt%)	Ni (Wt%)	Cu (Wt%)
25	ST01/01	1.684	7.316	28.654	0.062	0.159	0.04	0.515	0.007	0.013	0.152	0.103	18.008	0.008	11.926	31.353
26	ST01/02	2.252	5.62	32.153	0.207	0.43	0.028	0.556	0.159	0.013	0.148	0.158	15.935	0.007	10.244	32.09
27	ST01/03	5.011	3.487	32.063	0	0.036	0.23	0.515	0.366	0.012	0.1	0.159	22.81	0.008	7.595	27.608
28	ST35/01	1.694	3.046	31.351	0	0.038	0.785	0.565	0.529	0.008	0.104	0.006	19.97	0	9.095	32.809

Figure 13. Grey Basalts in the north eastern part of the area. The hammer handle (30 cm) is used as the scale.

Figure 14. Olivine Basalts. The hammer handle (30 cm) is used as the scale.

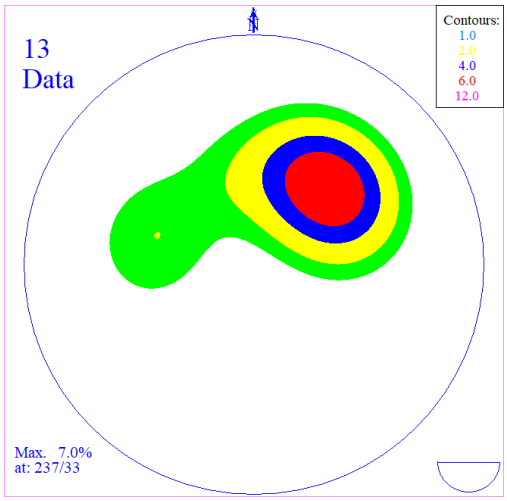

Figure 15. Contoured diagram of the poles in Korr-Marsabit area.

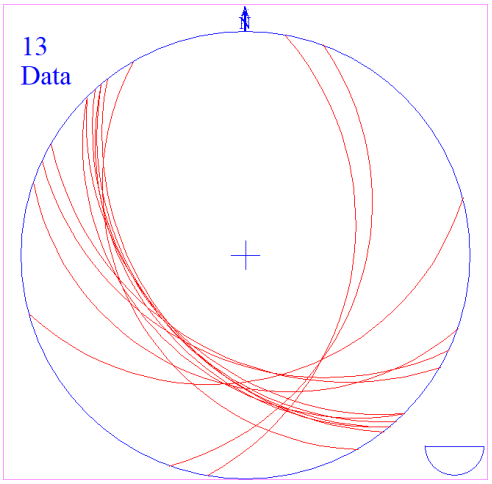

Figure 16. Diagram of the great circles showing that most of the limbs dip in the Southwest direction.

Geochemical Results and Discussion

The aim of geochemical survey and analysis was to establish the new elements associated with copper ore which could be identified physically. A total of 24 samples were prepared and analysis of major and trace elements was done using XRF prior to Krigging (**Table 4**) and another set of 5 samples (**Table 5**) analysed after kriging. Elements analysed included magnesium, calcium (CaO), potassium (K_2O), silica (SiO_2), phosphate (P_2O_5), sulphur (S), nickel (Ni), iron (Fe), chromite (Cr), vanadium (V), manganese (Mn), titanium (Ti), cobalt (Co), and copper (Cu). The rocks samples showing the concentrations of the elements analysed is tabulated in **Table 4** and **Table 5**. Some of these elements and their distribution in the area are shown in **Figures 18-20** under kriging subsection.

High concentration of copper (Cu), Nickel (Ni), Iron (Fe), Manganese (Mn), Titanium (Ti) and chromite (Cr) were found in the area. Samples BR/002A, BR/002B and BR/002E shows high concentration of copper (Cu), Nickel (Ni), Iron (Fe), and Magnesium. The location where these samples were collected is indicated on sampling map. BR/004A, BR/004AB and BR/021 indicate high concentration of chromite and titanium. Most of the rocks sampled in the area are enriched with titanium.

5. Elemental Association of Cu-Ni-Fe and Their Correlation with Other Elements

Mathematical considerations is used to determine the degree of interrelationship between the variables (Roonwal [18]; Annels [19]; Readdy *et al.*, [20]; Ali Akbar [21]). This relationship can be expressed by a mathematical expression, the correlation coefficient. The formula for this is as follows:

$$r = \frac{n\sum xy - \sum x \sum y}{\sqrt{\left[n\sum x^2 - \left(\sum x\right)^2\right]\left[n\sum y^2 - \left(\sum y\right)^2\right]}} \quad (1)$$

where;

X and Y are variables,

n is the number of observations,

r is the linear correlation coefficient.

Copper shows strong positive correlation with Nickel and Iron (Figure 17). This shows that the mode of delivery of this element could have been the same. The condition was favorable and allowed equilibrium stage to be reached to enable accumulation of this element in the system. It is also observed that copper has negative or null correlation with other elements. Weak correlation of copper and chromite is of great interest. This shows that the equilibrium for the formation of the two minerals in the area was not attained. It is however observed that chromite and cobalt have moderate correlation. This indicates that their mode of the delivery into the system was closely related.

6. Estimation of the Grades Using Kriging

Discontinuous kriging was used to make estimates of the Cu, Ni, and Fe grades of ore in sampled areas (Figures 18-20). This was due to absence or inadequacy of data within the area. Influence of each sampled point to the neighboring point is used (Roonwall, [18]).

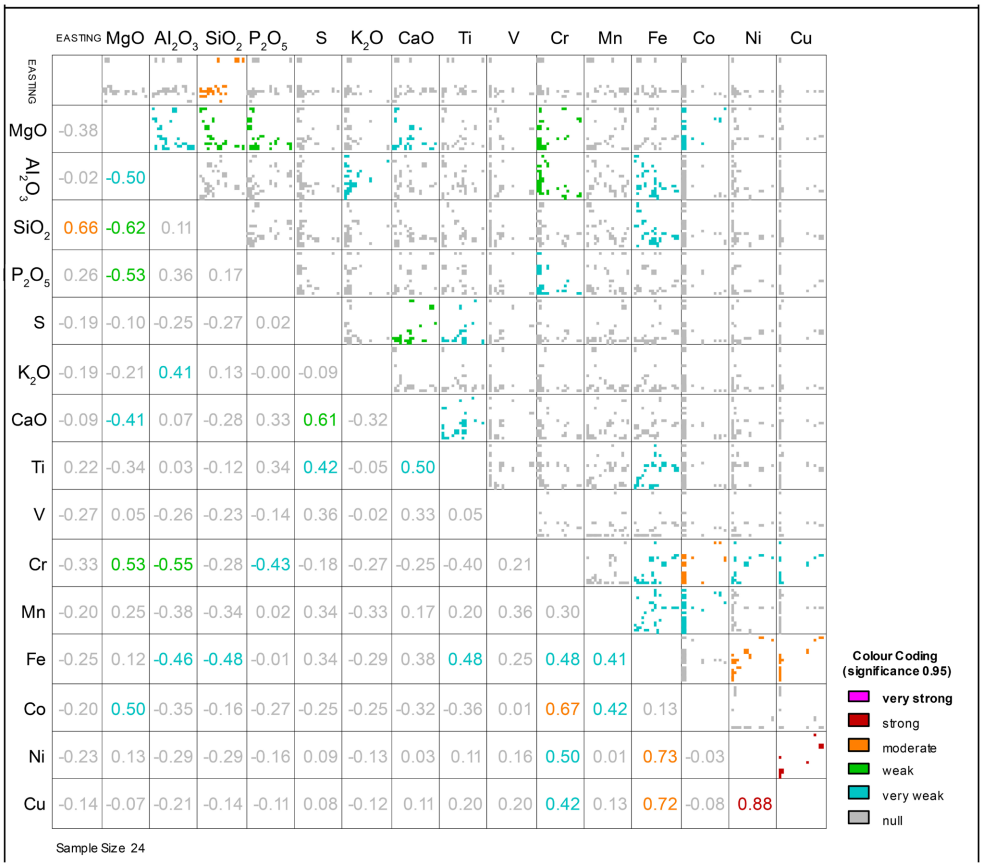

Figure 17. Correlation of element variation found in the rocks of Korr-Marsabit area, Northern Kenya.

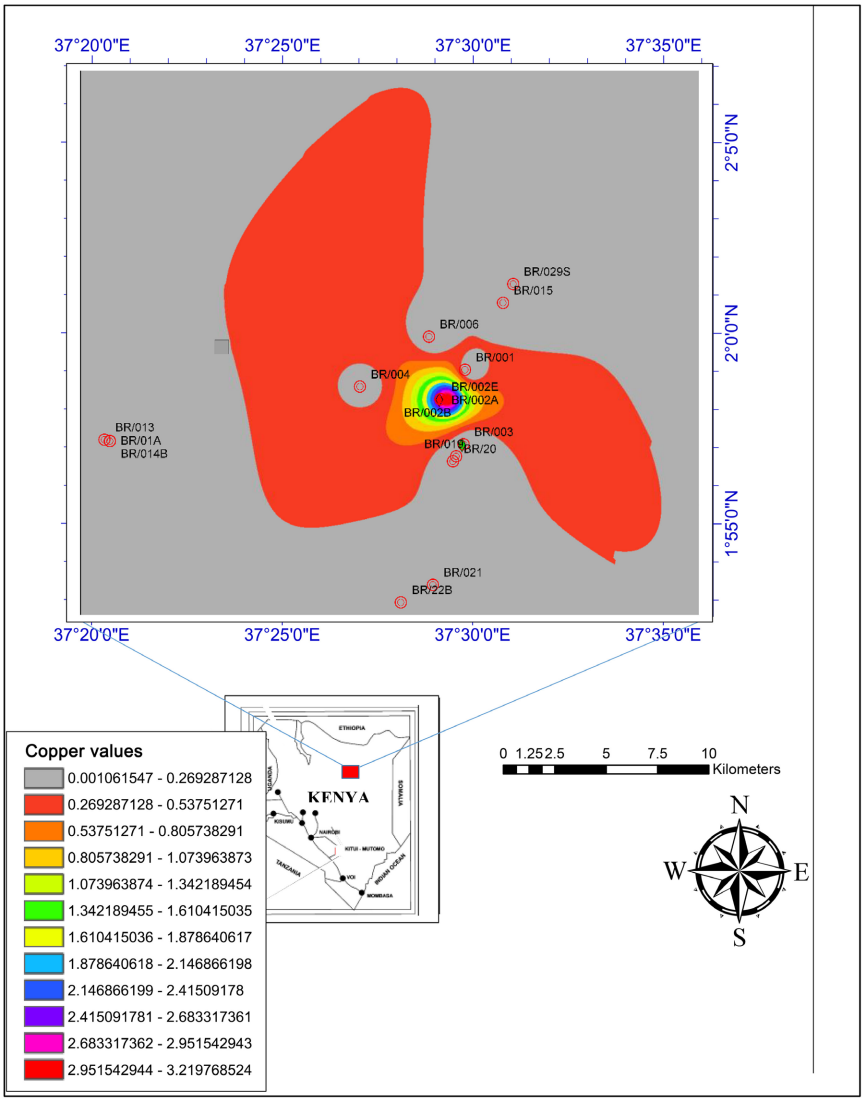

Figure 18. Estimated grade (%) Copper distribution in the Korr-Marsabit area, Northern Kenya.

The central point has an average grade of u, the first ring of point has an average weighted grade of v and the outermost ring of point an average weighted grade of w. An estimator z = 4 is made use of to predict the grade of the area. The estimator z is known as the Krigged estimator. Statistical tool on ArcGIS was used for this purpose and the plots of **Figures 18-20** were obtained with varying grades of Copper, Nickel and Iron.

7. Copper Ore Mineralization

Malachite is hosted in the gneisses, at an outcrop about 400 m South of Tirrim Upper Primary School (Sample No. ST01/01, ST01/02, ST01/03) and at an outcrop East of Bur Aramia hill (Sample no. ST35/01, ST35/02). The host rock is disseminated with both Malachite and Azurite. The sample in **Figure 21** was obtained from a pit of one meter deep.

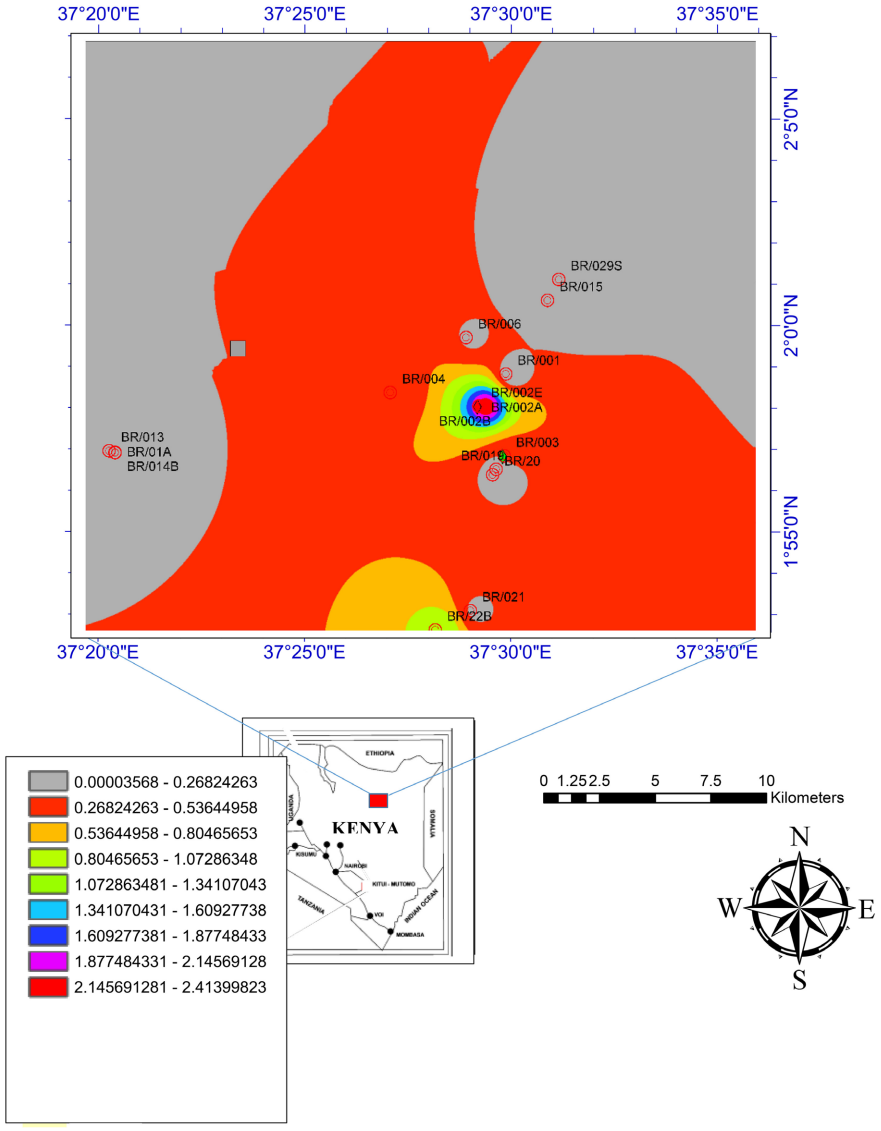

Figure 19. Estimated grade (%) of Nickel distribution in the Korr-Marsabit area, Northern Kenya.

8. Conclusion

Copper-nickel-iron are very important ore minerals in the current world and make a significant contribution to the economy. Understanding the genesis and ore association is of great importance to any exploration geologist. The main contribution of this research is correlation diagrams for elements indicating the hydrothermal/metamorphogenic ore genesis for Cu-Ni-Fe deposit occurring in the Korr-Marsabit area within the gneisses. It is through the use of these diagrams that we are able to understand the genesis of the ore minerals being explored. Elements (Ni and Fe) which have strong correlation with Cu formed during the same episode or were preserved in the malachite by direct substitution. This reactions were facilitated by temperature, pressure and sulphide fluids. The amphibolite facies metamorphism provided equilibrium for this substitution. Structural data have shown that the area has undergone deformation which

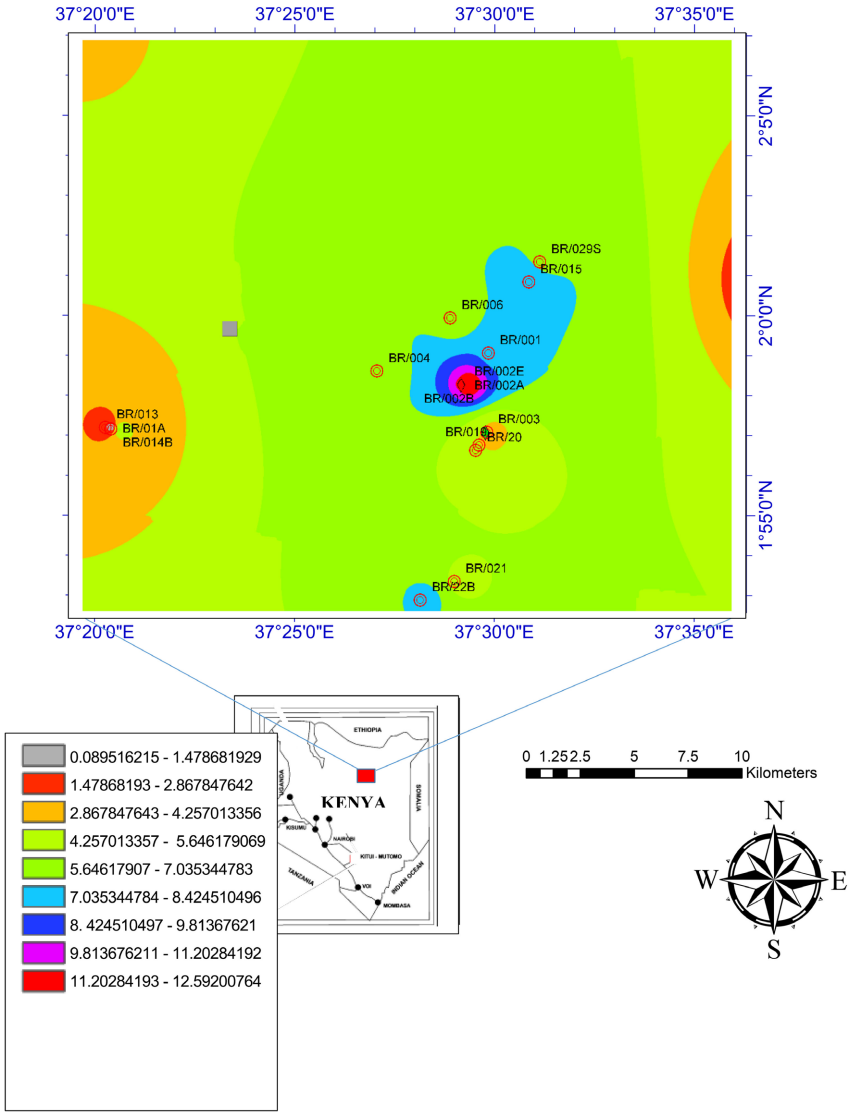

Figure 20. Estimated grade (%) Iron distribution in the Korr-Marsabit area, Northern Kenya.

Figure 21. Copper samples from Aramia hill. The pencil is (20 cm) is used as the scale.

could have contributed to medium-high grade metamorphism. Metamorphic rocks contain mineral assemblages that characterises the region to be amphibolite facies. It has also been shown that geostatistical tools can efficiently be used to predict extend of mineralization during exploration. Petrological study indicates that Korr-Marsabit area is an ophiolite suite which has been dismembered.

Conflicts of Interest

The author declares no conflicts of interest regarding the publication of this paper.

References

[1] Charsley, T. (1985) The Geology of Sheet 662 (Korr). Kenya Mines and Geology Dept., Nairobi.

[2] Key, R. (1987) Geology of Marsabit Area, Report 108. Ministry of Environment and Natural Resources, Nairobi.

[3] Stern, J.R. (1994) Arc Assembly and Continental Collision in the Neoproterozoic East African Orogeny: Implication for the Consolidation of Gondwanaland. *Annual Review of Earth and Planetary Sciences*, **22**, 319-351. https://doi.org/10.1146/annurev.ea.22.050194.001535

[4] Key, R., Charsley, T., Hakman, B., Wilkinson, A. and Rundle, C. (1989) Superimposed Upper Proterozoic Collision Controlled Orogenies in the Mozambique Belt of Kenya. *Precambrian Research*, **44**, 197-225. https://doi.org/10.1016/0301-9268(89)90045-4

[5] Waswa, A.K., Nyamai, C.M., Mathu, E.M. and Ichang'i, D.W. (2015) Petrology and Iron Ore Mineralization in the Neoproterozoic Mozambique Belt Rocks of Mutomo-Ikutha Area, S.E. Kenya. University of Nairobi, Nairobi.

[6] Mathu, E.M. (1992) The Mtito and Ikoo Faults in the Pan African Mozambique Belt, Eastern Kenya. In Mason, R., Ed., *Basement Tectonics* 7, Kluwer Academic, Dordrecht, 61-69. https://doi.org/10.1007/978-94-017-0833-3_5

[7] Mathu, M.E. (2000) Petrology and Tectonic Evolution of Archean and Neoproterozoic Rocks of Kakamega-Kapsabet Belt Area, Western Kenya. University of Nairobi, Nairobi.

[8] Mathu, M.E., Ngecu, W.M., Nyamai, C.M. and Davies, T.C. (1991) Proterozoic Island Tectonism in the Kenyan Mozambique Belt East of Nairobi. In: Muhongo, S., Ed., *Proceedings of the International Geological Field Conference on the Mozambique Belt in East Africa*, UNESCO, Tanzania, Vol. 8, 59.

[9] Nyamai, C.M., Mathu, M.E. and Ngecu, W.M. (1993) A Review of the Geology of the Mozambique Belt in Kenya. *Regional Trends in African Geology*: *Proceedings of the* 9*th International Geological Conference of the Geological Society of Africa*, Accra, 334-347.

[10] Nyamai, C.M., Mathu, E.M., Opiyo-Akech, N. and Wallbrecher, E. (2003) A Reappraisal of the Geology, Geochemistry, Structures and Tectonics of the Mozambique Belt in Kenya, East of the Rift System. *African Journal of Science and Technology Science and Engineering*, **4**, 51-71. https://doi.org/10.4314/ajst.v4i2.15306

[11] Clark, I.A.J. (1972) The Distribution of Fe and Ni between Synthetic Olivine and Sulfide at 900 Degrees Celcius. *Economic Geology*, **67**, 939-952. https://doi.org/10.2113/gsecongeo.67.7.939

[12] Clark, L.J. (1973) New Data on Phase Relations in the Cu-Fe-S Systems. *Economic Geology*, **68**, 443-454. https://doi.org/10.2113/gsecongeo.68.4.443

[13] Distler, W. and Genkin, A.D. (1980) Deposits of Sulfide Copper-Nickel Ores of USSR and Their Connection with Craton Volcanism. 6*th AGOD Symposium*, Stuttgart, 275-295.

[14] Distler, V.V., Genkin, A.D. and Dyuzhikov, A.O. (1986) Sulfide Petrology and Genesis of Copper Nickel Ore Deposits. In: Fredrich, G.H., Genkin, A.D., Naldrett, A.J., Ridge, J.D. and Sillitoe, R.H., Eds., *Geology and Metallogen of Copper Deposits*, Vol. 4, Springer, Berlin, 111-123. https://doi.org/10.1007/978-3-642-70902-9_7

[15] Ngecu, W.M. and Waswa, A.K. (2015) Global Tectonics "SGL 305 Lecture Series". University of Nairobi, Nairobi.

[16] Mehnert, K.R. (1968) Migmatites and the Origin of Granitic Rocks. Elsevier, Amsterdam.

[17] Biyajima, K., Suswa, K. and Miyakawa, K. (1975) Mantled Gneiss Dome in the Mozambique Belt around Machakos Area, Kenya. Preliminary Report, Nagoya University, Nagoya.

[18] Roonwal, G.S. (2018) Mineral Exploration: Practical Application. Springer, Berlin. https://doi.org/10.1007/978-981-10-5604-8

[19] Annels, A.E. (1991) Mineral Deposit Evaluation: A Practical Approach. Chapman & Hall, London, 436.

[20] Readdy, L.A., Bolin, D.S. and Mathuson, G.A. (1982) Ore Reserve Calculation. In: Hustrulid, W.A., Ed., *Underground Mining Methods Handbook*, Society of Mining Engineers, New York, 17-38.

[21] Ali Akbar, A. (2015) Application of Median Indicator Kriging in the Analysis of an Iron Mineralization. *Arabian Journal of Geosciences*, **8**, 367-377. https://doi.org/10.1007/s12517-013-1093-0